scientific reports

Check for updates

OPEN

Carbon cloth surface engineering for simultaneous detection of ascorbic acid, dopamine, and uric acid in fetal bovine serum

Lijun Bian✉, Xinglin Su & Jialu Wang

Carbon cloth (CC) was electrochemically activated using three electrochemical methods in different electrolytes. The gases released during the activation process etched the surface of the CC, thereby increasing its surface area of the activated CC (FCC). Moreover, functional groups such as oxygen-containing groups and N-doping have been introduced. The quantity and type of functional groups introduced during the activation process were related to the anions in the solution. FCC electrodes were used to construct electrochemical sensors for the simultaneous determination of ascorbic acid (AA), dopamine (DA), and uric acid (UA). The PFCC electrode activated by advanced cyclic voltammetry in $(NH_4)_2HPO_4$ showed linear ranges for AA, DA, and UA concentrations of 0.1 to 2.1 mM, 0.5 to 11 µM, and 0.5 to 11 µM, respectively. The detection limits are 72.93, 0.22, and 0.42 µM, respectively. The good flexibility the PFCC electrode made it suitable for the preparation of flexible sensors. The simultaneous determination of AA, DA, and UA in fetal bovine serum showed a reliable recovery ratio. This study provides a simple and green approach for activating carbon cloth and constructing flexible electrochemical sensors with the potential to simultaneously detect AA, DA, and UA.

Keywords Ascorbic acid, Carbon cloth, Dopamine, Simultaneous determination, Uric acid

Ascorbic acid (AA), dopamine (DA), and uric acid (UA) are essential organic substances that maintain human activity. AA is an antioxidant used to treat scurvy and low AA levels can lead to anemia and other diseases[1,2]. DA is the most abundant catecholamine neurotransmitter in the brain and its low levels can cause many neurological diseases[3,4]. UA is the final product of purine metabolism, and excessive UA can lead to gout[5,6]. Monitoring their contents is of great significance to human health[7]. Spectrophotometry[8], fluorescence[9], and electrochemical sensors[10,11] have been adopted for the detection of AA, DA, and UA.

Electrochemical sensors have attracted significant attention because of their simplicity and excellent sensitivity. However, owing to the overlapping voltammetric responses of AA, DA, and UA, distinguishing their coexistence in biological matrices remains challenging. Many electroactive materials have been used to modify traditional electrodes, including metal oxides[10,12], carbon nanomaterials[13–15], and other materials[16,17]. Among these electroactive materials, carbon is considered to be the most promising electrode material because of its natural abundance, low fabrication cost, and chemical stability. Moreover, the electrocatalytic activity, conductivity, and electrolyte affinity of carbon materials can be tailored by doping with heteroatoms, such as N, O, and S[18]. Owing to their excellent properties, carbon materials have been extensively used in energy storage and conversion devices[19], photocatalysis[20], and electrochemical catalysis[21].

Flexible electrochemical sensors have flexible substrates that can overcome the brittleness of traditional rigid electrochemical sensors. Thus, they are promising candidates for use in wearable devices[22,23]. The primary components of flexible electrochemical sensors are the flexible substrates and active materials[24]. Polymers and carbon materials are commonly used as flexible substrates. Various materials, including carbon materials[24], polymers[25], and metal compounds[26] have been employed as active components in the fabrication of flexible sensors. Most flexible electrochemical sensors are manufactured by depositing the active material onto the surface of a flexible substrate, which is a tedious process. The adhesion between the active material and flexible substrate significantly influences its performance. Carbon cloth (CC) is a low-cost conductive fabric composed of numerous uniform carbon microfibers. Although CC has excellent mechanical flexibility, strength, and good application prospects in flexible electrochemical sensors, little attention has been paid to it. The hydrophobicity and small specific surface area of carbon cloth hinder its application in electrochemistry[27]. Efforts have been

Department of Chemistry, Northeastern University, Shenyang 110819, China. ✉email: bianlijun@mail.neu.edu.cn

made to activate the CC to improve its electrochemical performance[28,29]. High-temperature annealing affords CC a larger hydrophilic surface, more functional groups, and excellent electrocatalytic performance for the reduction of imidacloprid[27]. A two-step reduction process after chemical exfoliation was used to activate CC. The formation of exfoliated carbon fiber structures on the surface of the carbon fibers increases the surface area[28].

Compared with previous activation methods, electrochemical methods eliminate the use of strong oxidants, have a controllable electromotive force, and are simpler, more effective, and more cost-effective. Activated CC obtained through electrochemical oxidation in a mixed acid solution exhibited excellent capacitive performance. The increase in pseudocapacitance was due to the enhancement of the surface area and functional groups[30]. In our previous study, we activated CC at a constant potential in a solution containing NH_4NO_3. Oxygen-containing groups and doped nitrogen were introduced onto the surface of the activated CC. It is unclear whether the doped nitrogen originates from ammonium or nitrate ions[31]. This study further investigated the effects of electrochemical methods and electrolytes on the type and quantity of functional groups during the activation process. The advanced cyclic voltammetry (CVA) method introduced the most functional groups and largest surface area. Different doping atoms were introduced when different electrolytes were used. The PFCC electrode obtained by CVA treatment in $(NH_4)_2HPO_4$ solution had a large surface area, abundant oxygen-containing groups, doped N, and doped P. The high surface area and functional groups provide numerous active sites to catalyze the oxidation of AA, DA, and UA. The superior catalytic properties and flexibility of the PFCC electrodes make them highly suitable for the development of flexible sensors that do not require additional substrates. This environmentally sustainable activation method represents a novel approach for the fabrication of flexible sensors. The simultaneous determination of AA, DA, and UA in fetal bovine serum (FBS) showed a reliable recovery ratio.

Experimental

Reagents and materials

AA, DA, and UA were obtained from the Aladdin Biochemical Technology Co. Ltd. (Shanghai, China). All other reagents were of analytical grade and used without further purification. FBS was purchased from Sangon Biotech Co., Ltd. (Shanghai). Phosphate buffer solutions (PBS) were prepared from Na_2HPO_4 and NaH_2PO_4. CC was obtained from Fuel Cell Earth LLC (USA) and washed thoroughly with acetone and deionized water before electrochemical activation.

Electrochemical activation of carbon cloth

Three electrochemical methods were used to activate CC. Method 1 is CVA. Ten cyclic voltammetry scans were conducted in 1 M solutions of $(NH_4)_2SO_4$, $(NH_4)_2HPO_4$, and NH_4Ac between − 1.9 to 1.9 V (vs. SCE), with each scan held at 1.9 and − 1.9 V for 1 min, respectively. The activated CC electrodes were denoted as SFCC1, PFCC, and AFCC. In methods 2 and 3, CC electrodes were activated through anodic or cathodic electrolysis at + 1.9 V and − 1.9 V in 1 M $(NH_4)_2SO_4$ for 10 min. The activated CC electrodes were denoted as SFCC2 and SFCC3.

Characterization

The surface morphologies were analyzed using a Hitachi SU-8010 field-emission scanning electron microscope (FE-SEM, Japan). The surface elemental composition of FCCs was investigated by X-ray photoelectron spectroscopy (XPS) (ESCALAB 250Xi, Thermo Scientific Escalab, USA). Contact angles were evaluated using a contact angle meter (KRUSS DSA25, Germany), and material hydrophobicity was assessed using deionized water droplets.

Results and discussion

Effect of electrochemical methods

The morphologies of the CC and SFCC electrodes are shown in Fig. 1. The surface of the CC was smooth and flat, with few cracks. The number of cracks on the surface of SFCC3 was comparable to that on the surface of CC but fewer than those on the surfaces of SFCC1 and SFCC2. The cracks on the surface of SFCC2 were wider and deeper than those on SFCC1 and SFCC3. This is related to the different electrochemical reactions that occurred during the three activation processes. During the activation process of SFCC3, the electrode potential is lower than the hydrogen evolution potential, and the hydrogen evolution reaction (HER) hinders the intercalation of cations into the graphite layers[32]. The reaction mainly occurred on the surface and the released H_2 etched the CC surface, resulting in fewer cracks. During the activation process of SFCC2, hydroxyl (OH·) and oxygen radicals (O·) produced by water oxidation hydroxylate or oxidize the surface of CC, resulting in the formation of oxygen-containing functional groups, such as hydroxyl (C–OH) carbonyl (C = O) and carboxylic acid (COO^-) groups[33,34]. At the same time, the oxidation of CC at the edges and defects reduces the van der Waals force between the graphite sheets and facilitates the insertion of sulfate ions and water into the graphite layer[34,35]. Hence, oxygen evolution occurred not only on the surface of the carbon fiber but also at the inner site, and the released O_2 gases caused some graphite to fall off the surface of SFCC2, leading to more and wider cracks on the surface of SFCC2. In the activation process of SFCC1, redox reactions occur alternately on the electrode surface. The oxidized CC was reduced during the cathode process; therefore, fewer sulfate ions and water were inserted into the graphite layer, resulting in fewer and narrower cracks than those on SFCC2, and the degree of oxidation of SFCC1 was lower than that of SFCC2. The cracks on the surface of the SFCC electrodes increased their surface areas. The increased surface area provides more active sites for catalysis, thereby enhancing the electrocatalytic performance of the SFCC electrodes towards CC. The electrochemically active areas of the CC

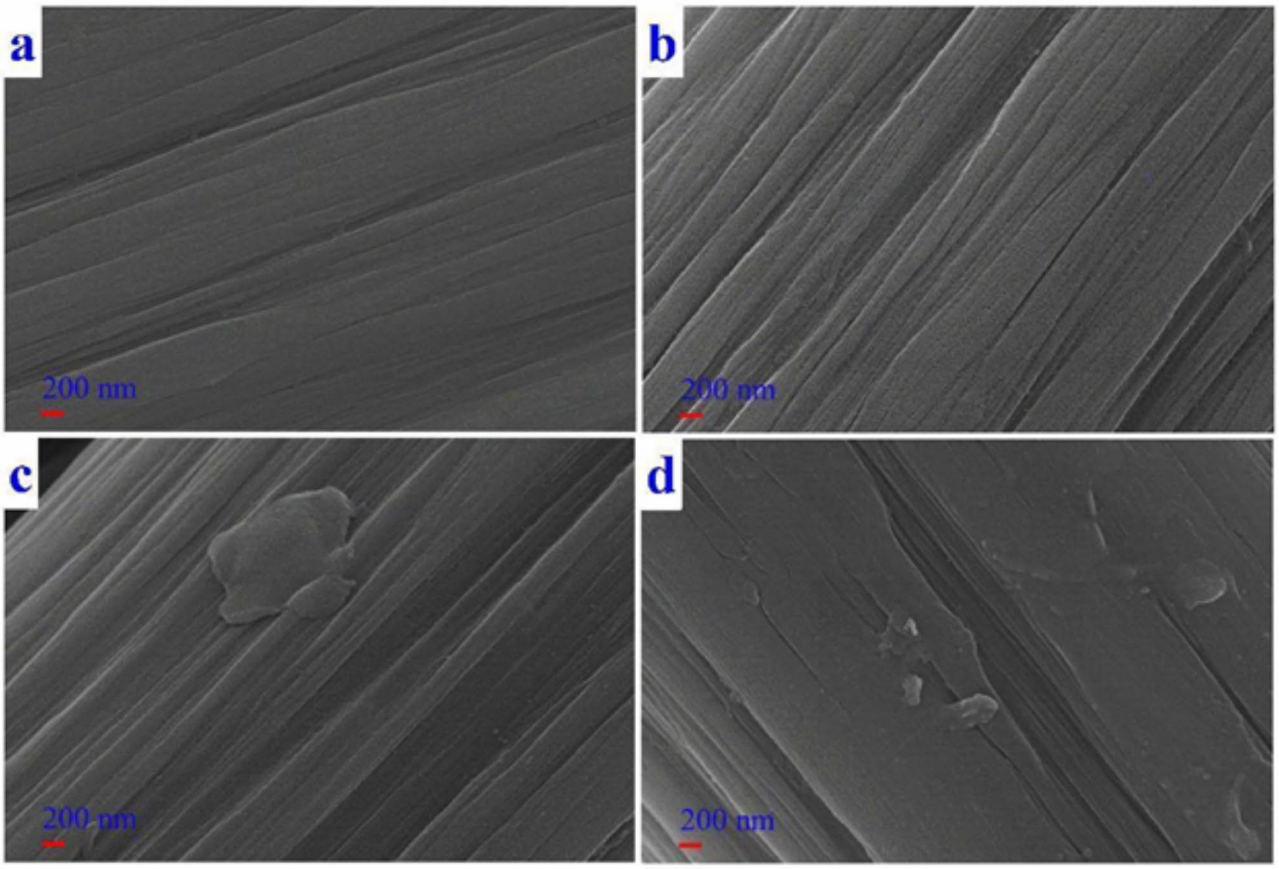

Fig. 1. SEM images of CC (a), SFCC1 (b), SFCC2 (c), and SFCC3 (d) electrodes.

	C%	*N*%	O%	S%
CC	90.91	1.14	7.95	/
SFCC1	66.41	2.17	29.27	2.15
SFCC2	54.86	2.33	39.56	3.24
SFCC3	87.02	1.30	11.68	0.20

Table 1. Surface composition of CC and SFCC determined by XPS (at%).

and SFCC electrodes calculated using the Randles-Ševčík equation (i_{pc} =(2.69×10^5) n$^{3/2}$ D$^{1/2}$ v$^{1/2}$ A c) were 0.037, 0.132, 0.083, and 0.041 cm^2, respectively.

XPS was used to compare the type and quantity of functional groups introduced during the activation process. The atomic percentages of these materials are listed in Table 1. CC contains 1.3% N because the raw material for preparing CC is polyacrylonitrile. After activation, the oxygen contents of SFCC1 and SFCC2 significantly increased, whereas that of SFCC3 did not change significantly. The S element appeared on the surface of all SFCC electrodes. The introduction of S doping through electrochemical methods has been reported in the literature, in which N and S co-doped graphene was obtained by electrochemical exfoliation using $(NH_4)_2SO_4$ as the electrolyte[36,37]. The nitrogen content of SFCC1 was comparable to that of SFCC2 and higher than that of CC and SFCC3, indicating that N was introduced during the anodic activation process. N was introduced through condensation and amination reactions between the oxidation products of ammonia and oxygen-containing functional groups[38,39].

The high-resolution C 1s spectra are shown in Fig. S1 (Supplementary Information). It can be divided into four peaks, carbon sp2 bonds, C=C (284.7 eV), C-N/C-O/C-S (285.9 eV), carbonyl/quinone group, C=O (287.2 eV) and carboxylic group O-C=O (288.9 eV)[36,37,40]. The distributions of the oxygen-containing functional groups are summarized in Table 2. The sp2 hybrid carbon content was dominant in all the samples. The carboxylic groups were reduced during cathodic activation; thus, there were no carboxylic groups on SFCC3. More oxygen-containing functional groups are introduced during the anodic activation process. The number of oxygen-containing functional groups in SFCC1 and SFCC2 was much higher than that in CC and SFCC3. Owing to the reduction of some oxygen-containing groups introduced during the anodic process in

	Csp^2	C-O/C-*N*/C-S	C=O	O-C=O
CC	60.53	26.12	9.72	3.63
SFCC1	70.52	14.11	8.17	7
SFCC2	63.6	6.87	22.94	6.56
SFCC3	84.79	15.21	/	/

Table 2. Distributions of the oxygen-containing functional groups (%).

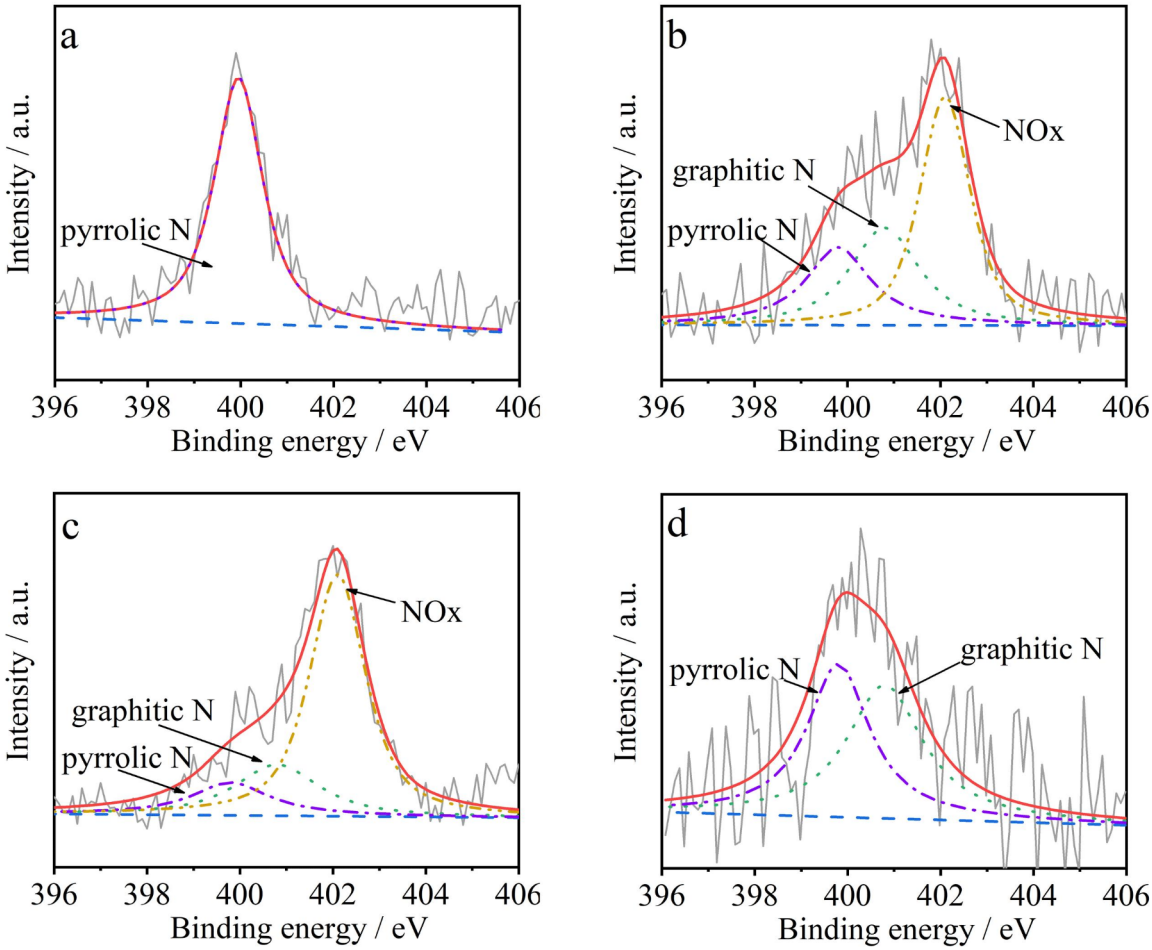

Fig. 2. N 1s high-resolution spectra of (**a**) CC, (**b**) SFCC1, (**c**) SFCC2, (**d**) SFCC3.

the cathodic step, the carbonyl/quinone group content in SFCC1 was lower than that in SFCC2. An appropriate number of oxygen-containing functional groups can improve the electrochemical activity, but a large number of oxygen-containing functional groups may destroy the π-π conjugate structure of graphite and reduce the carrier mobility and carrier concentration, thus reducing the conductivity of CC[41,42]. The electrochemical impedance results showed that SFCC2 had the lowest charge-transfer resistance (Fig. S2).

The amount of nitrogen in SFCC3 is comparable to that in CC, whereas the amount of nitrogen in SFCC1 and SFCC2 is higher than that in CC, which means that nitrogen can be introduced during the anodic activation process, but not during the cathodic activation process. The doping of electron-rich N atoms induces positive charge density redistribution on adjacent carbon atoms, which facilitates the chemical adsorption and charge transfer of the analyte, thereby enhancing the catalytic activity[43,44]. As shown in Fig. 2, the N 1s spectrum can be deconvoluted into pyrrolic N (399.8 eV), graphitic N (400.8 eV), and pyridinic N-oxide (NO_x) (402.1 eV)[35,45,46]. The configuration of nitrogen in CC is pyrrolic N, a portion of which is converted into graphite-N and pyridinic N-oxide after electrochemical activation. Graphitic-N promotes catalytic activity by reducing the absorbed energy and improving the electrical conductivity[43,44]. Pyridinic N-oxide (NOx) was observed in SFCC1 and

SFCC2, which may have been introduced during the oxidation-activation process. Because the oxidation reaction occurred throughout the entire activation process of SFCC2, both the oxidation and reduction reactions occurred during the activation process of SFCC1, and the NOx and oxygen contents of SFCC1 were lower than those of SFCC2. Pyridinic N-oxide can increase the hydrogen bonding between AA, DA, and UA molecules, thereby enhancing electrocatalytic activity[47].

The S 2p spectrum can be divided into four peaks: thiophene-S1/2 (164.9 eV), thiophene-S3/2 (166.1 eV), C-SO_x (168.6 eV), and C-SO_x (170 eV)[46,48] as shown in Fig. S3. The doped-S can accelerate the transfer of electrons to biomolecules, thereby improving electrocatalytic performance[48].

The surface of CC is hydrophobic, with a contact angle of 130° (Fig. 3a), which is related to hydrocarbon pollution in the air[49]. The contact angle of SFCC3, which was also hydrophobic, was 128°. The activation process may not be able to remove hydrocarbon contamination and introduce sufficient oxygen-containing groups, resulting in no improvement in the hydrophilicity of the SFCC3. Poor interface contact with the electrolyte can weaken electron transport on the electrode surface[46]. Figure 3b and c indicate that the wetting performance of carbon cloth was greatly improved. The gases released during the activation process, such as O_2, may etch the surface of CC, thereby removing hydrocarbon contamination. Oxygen-containing groups were also introduced during the activation process, leading to an improvement in hydrophilicity. The contact angle of SFCC2 was smaller than that of SFCC1, which was related to the presence of more oxygen-containing groups on the surface of SFCC2. Increasing the surface hydrophilicity can improve the electrochemical performance of the electrodes, as the electrochemical response largely depends on the adsorption and permeation of electrolytes on the electrode surface.

The CV curves recorded in the solutions containing 1 mM AA, 50 μM DA, and 100 μM UA are shown in Fig. 4a-c. The conversion of the hydroxyl groups to carbonyl groups in the furan ring of AA at all electrodes was irreversible. The oxidation potential of AA at SFCC1 shifted negatively to -24 mV, which is more negative than that of CC (20 mV), SFCC2 (4mV), and SFCC3 (-22 mV). The negative shift potential may be attributed to the high conductivity of graphitic-N as well as the increased number of active sites provided by pyridine nitrogen oxides and doped S[43,48]. The response current at SFCC1 was higher than those at SFCC1, SFCC3, and CC, which was related to its highest surface area, which is consistent with the previous SEM results. The responses of all electrodes to DA were similar and a well-defined redox couple was observed for all electrodes. The peak separations at the CC and SFCC electrodes were 41, 34, 23, and 36 mV, respectively. The smaller peak separation at SFCC was attributed to the interaction between the hydroxyl or amine groups in DA molecules and the nitrogen and sulfur atoms doped in SFCC through hydrogen bonds. The response current of DA at SFCC1 was the highest. The oxidation of UA at the CC was irreversible; in contrast, a reduction peak appears at the SFCC, indicating that the reaction reversibility of UA was promoted.

The oxidation peak of AA overlapped with that of DA on CC; therefore, there were only two oxidation peaks when the three components coexisted in solution (Fig. 4d), and the simultaneous detection of these three biomolecules at the CC electrode was impossible. In contrast, the oxidation potential of AA on SFCC decreased

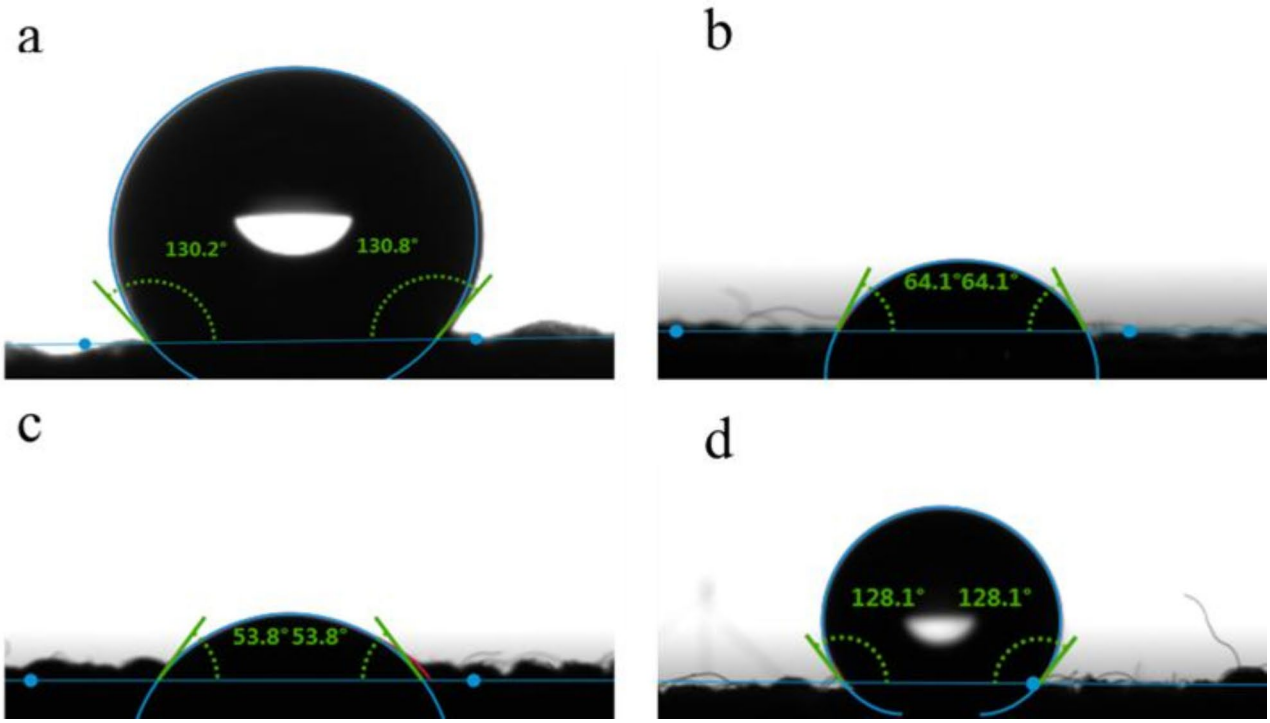

Fig. 3. The contact angles of water on (**a**) carbon cloth and (**b**) SFCC1, (**c**) SFCC2, (**d**) SFCC3.

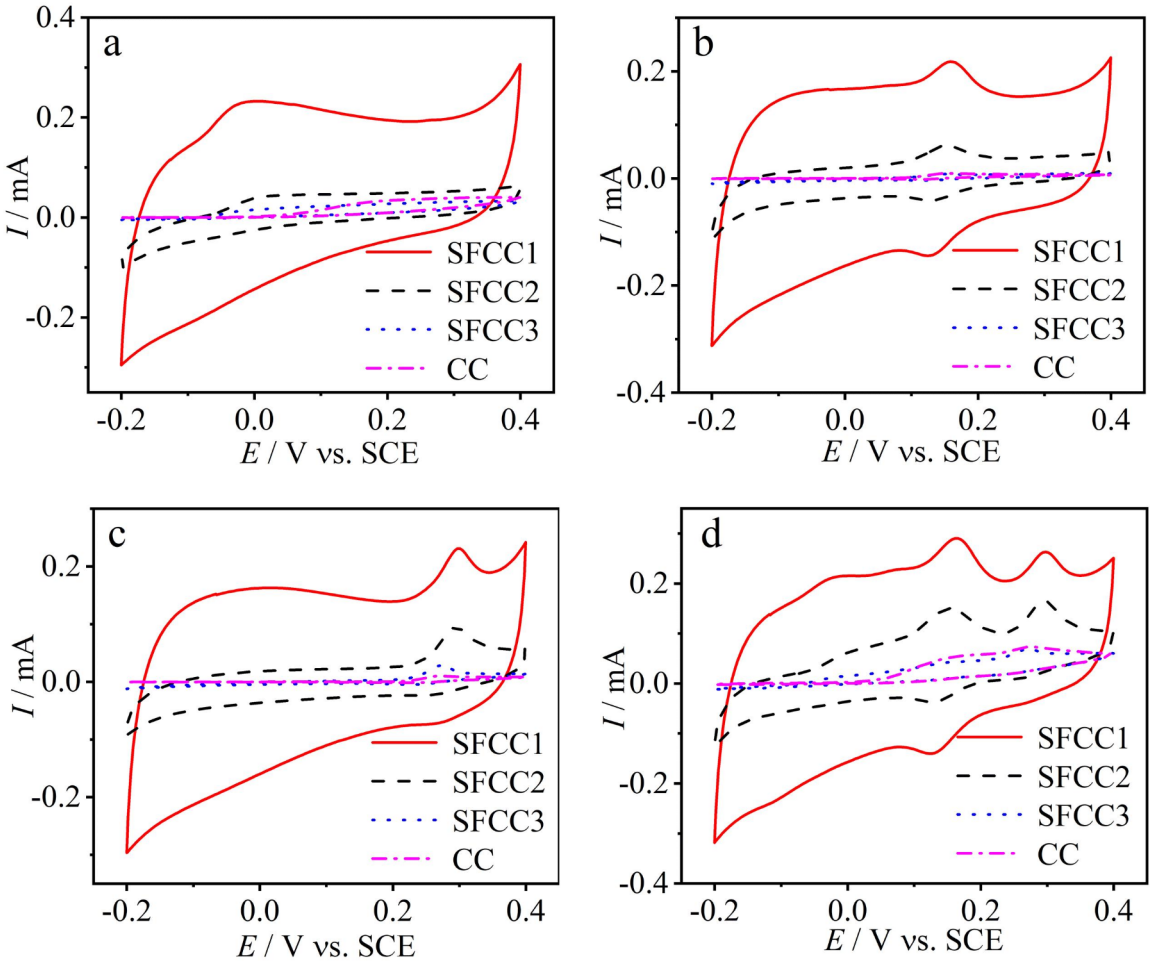

Fig. 4. CV response of CC and FCC electrodes in the solution containing AA (**a**), DA (**b**), UA (**c**), AA, DA, and UA (**d**).

to approximately 0 V; therefore, there were three oxidation peaks in all the CV curves of SFCC, which could achieve simultaneous detection. The oxidation currents of AA, DA, and UA at SFCC1 and SFCC2 were much higher than those at CC and SFCC3, which was attributed to the increase in surface area during the activation process, providing more active sites. The peak potential separation (ΔEp) between AA and DA in SFCC1 (188 mV) was larger than those in SFCC2 (145 mV) and SFCC3 (171 mV). The larger ΔEp and higher peak current indicate that SFCC1 exhibits excellent electrochemical performance and can be used for the simultaneous determination of AA, DA, and UA. The excellent electrochemical performance of SFCC1 may be attributed to the following factors: (i) The high surface area caused by the activation process provides a large number of active sites, and (ii) Doping with N and S provides more active sites, alters its electronic structure, and enhances its conductivity.

The influence of electrolytes on electrocatalytic performance

Based on the above results and discussion, the cathodic activation process cannot increase the active area of SFCC3 nor can it introduce doped N. Consequently, SFCC3 exhibited poor electrochemical sensing performance. Not only oxygen-containing groups but also doping-N and S can be introduced by the anodic activation process. Excessive oxygen-containing functional groups disrupt the conductivity of SFCC2, leading to a decrease in the electrocatalytic performance. The CVA activation process involves anodic and cathodic electrolysis, and doping-N, doping-S, and oxygen-containing functional groups can be introduced during this process. The conductivity of SFCC1 is superior to those of SFCC2 and SFCC3, and the electrochemically active area of SFCC1 is larger than those of SFCC2 and SFCC3, which makes SFCC1 has the best electrochemical sensing performance. The CVA activation process is superior to single anodic and cathodic activations. Activate CC with CVA in different ammonium salt solutions to further investigate the effect of electrolytes on the type and quantity of functional groups and the electrochemical performance.

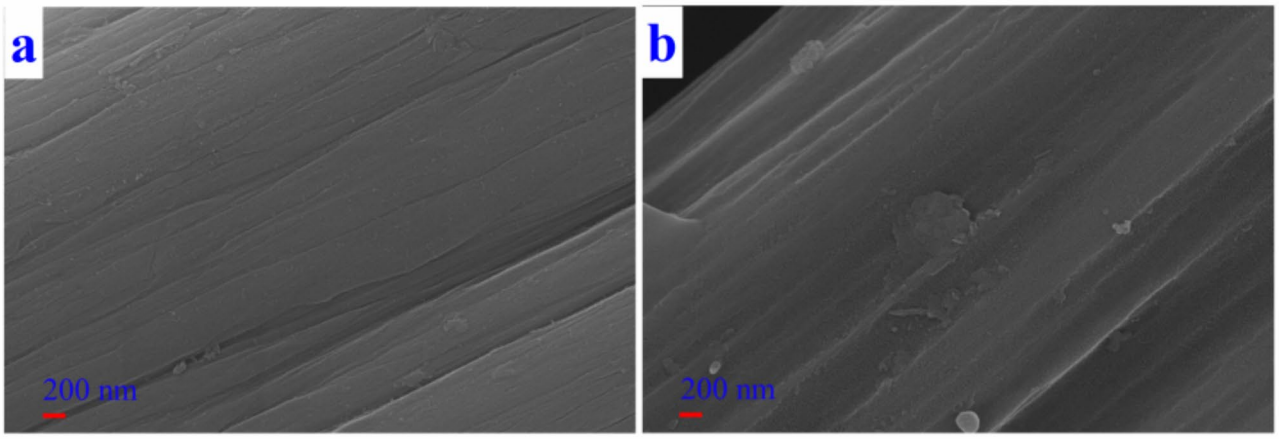

Fig. 5. SEM images of AFCC (**a**) and PFCC (**b**).

	C%	*N*%	O%	*P*%
PFCC	67.13	5.95	26.22	0.70
AFCC	84.56	1.77	13.67	/

Table 3. Surface element composition of PFCC and AFCC determined by XPS (at%).

The surface morphologies of PFCC and AFCC obtained via CAV activation in 1 M $(NH_4)_2HPO_4$ and NH_4Ac are shown in Fig. 5. The surface of AFCC was smooth, with a few shallow cracks. During the cathodic activation process, the HER hindered the intercalation of cations into the graphite layers; consequently, the HER mainly occurred on the AFCC surface. During the anodic activation process, the acetate ions were oxidized to CO_2 and could not be inserted into the graphite layer. Therefore, AFCC had few shallow cracks. The cracks on the surface of PFCC were deeper and wider than those on SFCC1. The radius of PO_4^{3-} is larger than that of SO_4^{2-}, which has a stronger wedge effect and is conducive to expanding the space between the graphite sheets and facilitating the entry of water and electrolytes[40]. The insertion of water and electrolytes causes graphite sheets to easily fall off the carbon fiber, leading to deep and wide cracks. The electrochemically active areas of the AFCC and PFCC electrodes calculated using the Randles-Ševčík equation were 0.079 and 0.053 cm^2, respectively.

The surface compositions of PFCC and AFCC, determined by XPS, are listed in Table 3. The nitrogen content of AFCC was slightly higher than that of CC and lower than those of SFCC1 and PFCC, indicating the introduction of a small amount of nitrogen. The nitrogen content of PFCC was much higher than those of SFCC1 and AFCC, indicating that the activation in phosphate can facilitate N doping. Phosphorous was observed on the surface of PFCC, indicating its introduction during activation. A similar electrochemical method was used to obtain N, P co-doped graphene in $(NH_4)_2HPO_4$ solution[33,37]; however, the doping mechanism is still unclear. The oxidation of acetate prevented the oxidation of CC, resulting in the oxygen content on AFCC being comparable to that of CC. The oxygen content of PFCC is lower than that of SFCC1 because phosphate can prevent the excessive oxidation of CC[40].

Figure 6 shows the high-resolution N 1s and P 2p spectra. The oxidation of acetate ions not only prevents the oxidation of CC but also prevents the formation of NOx. Doped nitrogen was present in the form of pyrrolic N and graphitic N in AFCC. The NOx content of PFCC was significantly lower than that of SFCC1, which can be attributed to the ability of $(NH_4)_2HPO_4$ to inhibit excessive oxidation of CC[40]. The high-resolution P 2p spectra could be fitted to P-C and P-O bonding configuration[43,50]. The main component of the P-C bond indicated the successful incorporation of P.

Fig. 7 shows the electrooxidation of AA, DA, and UA on PFCC and AFCC. The oxidation potentials of AA at AFCC and PFCC were − 49 and − 35 mV, respectively, which were more negative than those at SFCC1 (-24 mV). The oxidation potentials of UA at AFCC and PFCC were 28 and 26 mV, respectively, which were more negative than those at SFCC1 (30 mV). This may be attributed to the fact that the greatest number of negatively charged functional groups on the surface of SFCC1 hinders the oxidation of negatively charged AA (pKa = 4.4) and UA (pKa = 5.7) at the electrode surface. The peak separations of the DA redox couples at PFCC and AFCC were 20 and 24 mV, respectively which were smaller than those at SFCC1 (34 mV), indicating the best reversibility and highest electron transfer rate of the DA redox reaction at PFCC. This may be attributed to the large amount of doped N, which can improve its conductivity, activate the hydroxy and amine groups, and accelerate the charge transfer kinetics of DA at PFCC[51]. Meanwhile, doped P can improve the catalytic activity of the nitrogen atom active center[43,50]. The oxidation of AA was not obvious at AFCC when AA, DA, and UA coexisted; thus, it was not suitable for the simultaneous detection of AA, DA, and UA. The oxidation currents of AA, DA, and UA on SFCC1 were the highest, regardless of whether they existed alone or in combination. This was attributed to the

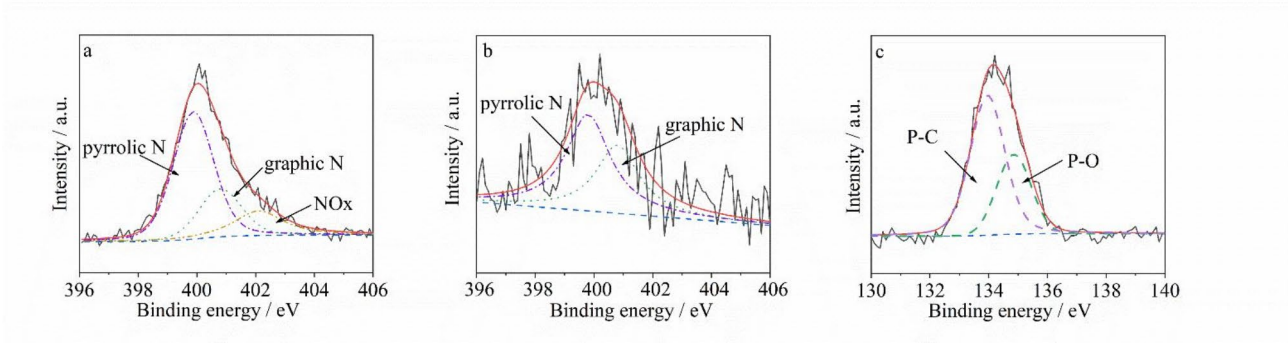

Fig. 6. N 1s high-resolution spectra of PFCC1 (**a**), AFCC (**b**), N 1s high-resolution spectra of PFCC (**c**).

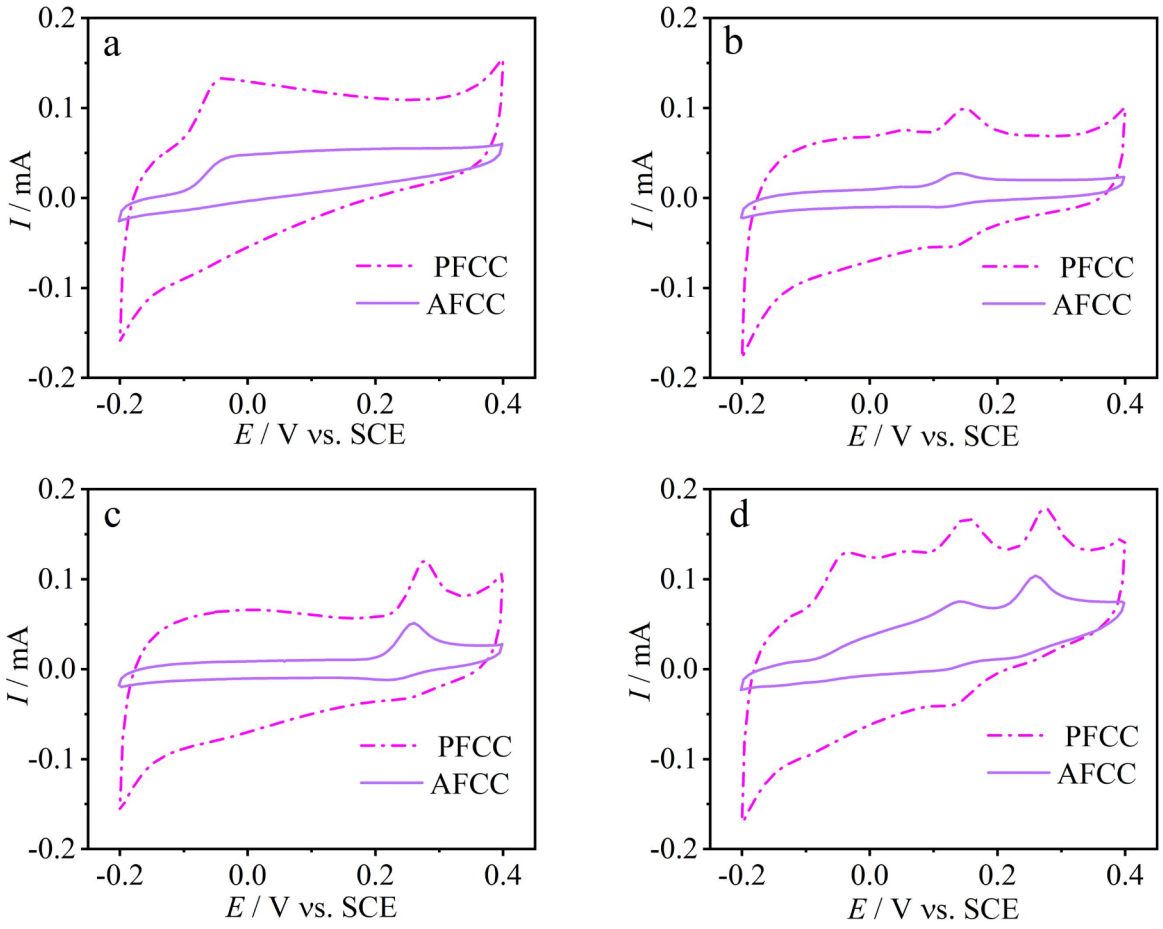

Fig. 7. CV response of AFCC and PFCC electrodes in the solutions containing AA (**a**), DA (**b**), UA (**c**), AA, DA, and UA (**d**).

fact that the maximum surface area of SFCC1 provided more active sites. The high surface area of SFCC1 also generated high capacitive current. The peak potential separations of AA-DA on SFCC1 and PFCC were 184 and 200 mV, and those of AA-UA were 321 and 331 mV, respectively. Considering both current and peak separation, PFCC was used to detect AA, DA, and UA in subsequent experiments.

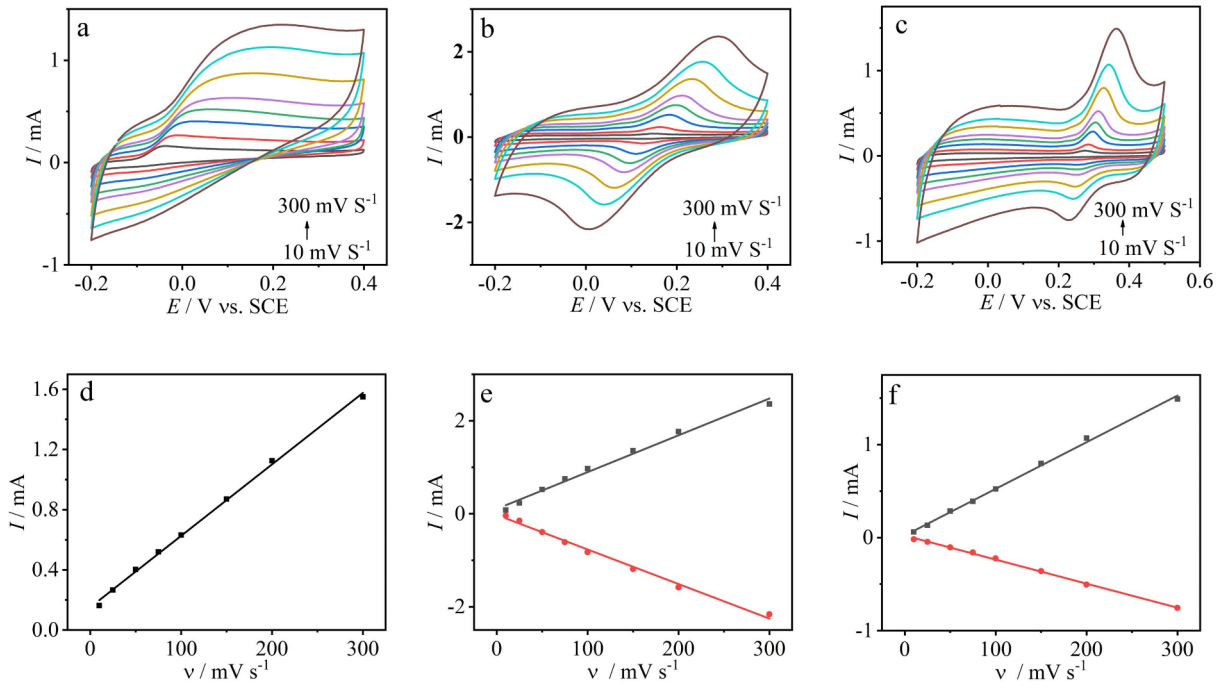

Fig. 8. CV curves of (**a**) 1mM AA, (**b**) 50 μm DA, (**c**) 0.1 mM UA on the PFCC electrode at different scan rates, 10, 30, 50, 100, 150, 200, 250, 300 mV s^{-1}, peak currents of (**d**) AA, (**e**) DA, (**f**) UA versus scan rates.

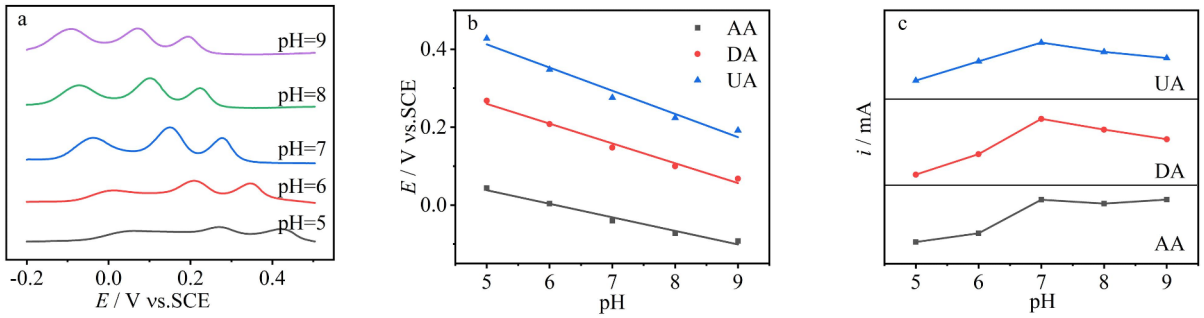

Fig. 9. (**a**) DPV curves of the PFCC electrode in PBS with different pH values; (**b**) pH dependence of formal potentials in DPV curves; (**c**) Relationship between peak currents and pH.

Effect of the scan rate and pH value

To further investigate the electrochemical behavior of AA, DA, and UA on PFCC, CVs were recorded at various scan rates, and the results are shown in Fig. 8a–c. As the scan rate increased, the peak current increased, the oxidation peak shifted positively, and the reduction peak shifted negatively. The relationships between peak currents and scan rates are shown in Fig. 8d–f. These values are proportional to each other, indicating that the oxidation reactions of AA, DA, and UA are controlled by surface adsorption[52,53].

To investigate the effect of pH on the electrochemical response of PFCC to AA, DA, and UA, differential pulse voltammetry (DPV) measurements were conducted in solutions with different pH values. As shown in Fig. 9a, the peak potential negatively shifted with increasing pH, indicating that protons were involved in the oxidation process[54]. The relationship between the peak potential and pH is shown in Fig. 9b. The slopes of the three linear regression equations were 31.8, 54.2, and 59.5 mV/pH respectively. According to the Nernst equation, Ep = (−0.0592 m/n) pH + b (where n is the electron transfer number and m is the number of protons)[55]. The slopes of

DA and UA were close to 59 mV/pH, indicating that their oxidative reactions were two-electron and two-proton processes. The slope of AA was below 59 mV/pH, indicating a single-proton and two-electron transfer process[56]. The response currents of AA, DA, and UA at different pH values are shown in Fig. 9c. The response current of the three substances is maximum at pH 7; therefore, subsequent experiments were conducted at pH = 7, which is also close to the pH value of human body fluid[57].

Simultaneous determination of AA, DA, and UA

DPV measurements were used to evaluate the electrochemical sensing performance of PFCC for AA, DA, and UA. Figure 10 shows the electrochemical response of PFCC to varying concentrations of AA, DA, and UA. The three separate peaks in the DPV curves correspond to the oxidation of AA, DA, and UA, respectively. The oxidation peak currents of AA, DA, and UA were proportional to their concentrations, ranging from 0.1 to 2.1 mM, 0.5 to 11 µM, and 0.5 to 11 µM, respectively. The detection limits were 72.93, 0.22, and 0.42 µM, respectively. Table 4 presents a comparative analysis of the analytical performance of the PFCC electrode and previously reported electrodes. PFCC demonstrated an electrochemical performance comparable to that of previously reported materials. Electrochemical activation offers precise control over the activation process, allowing the production of FCC electrodes with tunable properties. This method is environmentally friendly because it typically uses mild electrolytes, avoids harsh chemicals, and operates at room temperature and atmospheric pressure. Additionally, electrochemical activation is scalable and cost-effective, making it suitable for the large-scale industrial production of PFCC. Thus, the PFCC electrode showed potential for future use in electrochemical analytical applications.

Repeatability and stability

Repeatability was determined by recording eight DPV responses in a solution containing 2 mM AA, 10 µM DA, and 20 µM UA. The response currents to AA, DA, and UA remained almost unchanged, with relative standard deviations of response current are 0.53%, 0.78%, and 2.4%, respectively. After one week of storage in PBS, the

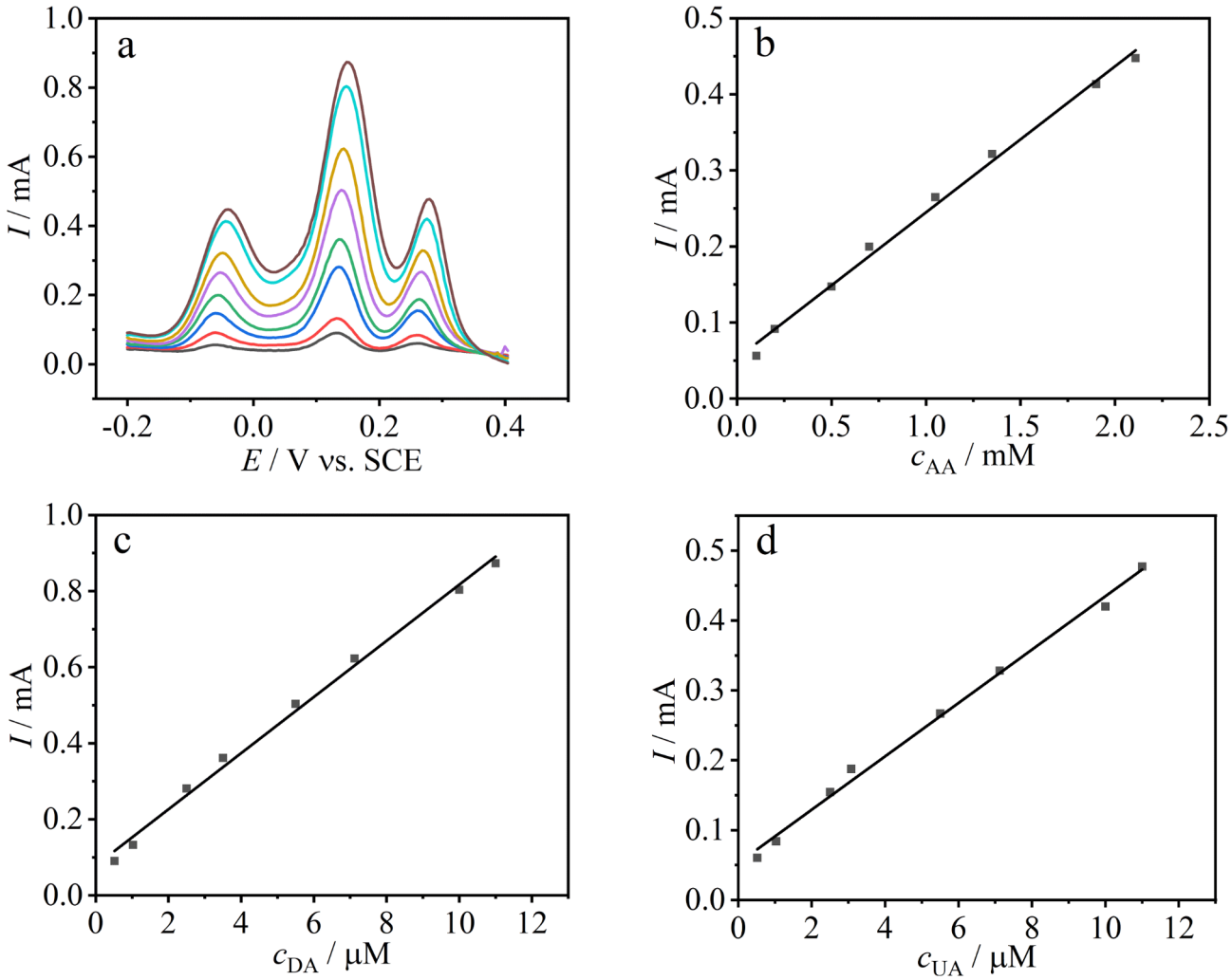

Fig. 10. (**a**) DPV curves of different concentrations of AA, DA, UA on the PFCC electrode in 0.1 M PBS; the calibration curves of the oxidation peak currents versus the concentrations of (**b**) AA, (**c**) DA, (**d**) UA.

Electrode	Linear range/μM			Detection limit/μM			Ref.
	AA	DA	UA	AA	DA	UA	
g-C_3N_4/MWNTs/GO	200–7500	2–100	4–200	96	0.22	1.36	[1]
ERGO/GCE	500–2000	0.5–60	0.5–60	250	0.5	0.5	[2]
LaV-MWCNTs	–	2-100	2-100	-	0.046	0.025	[5]
S-fs-ERG	2.5–40 40-1000	0.1–50	0.5–50	2.5	0.1	0.1	[7]
FCC2	100–4000	0.02-3	0.1–10	5.8	0.014	0.066	[31]
PFCC	1–2100	0.5–11	0.5–11	72.93	0.22	0.42	This work

Table 4. Comparison of electroanalytical parameters of different electrodes for simultaneous determination of AA, DA, and UA.

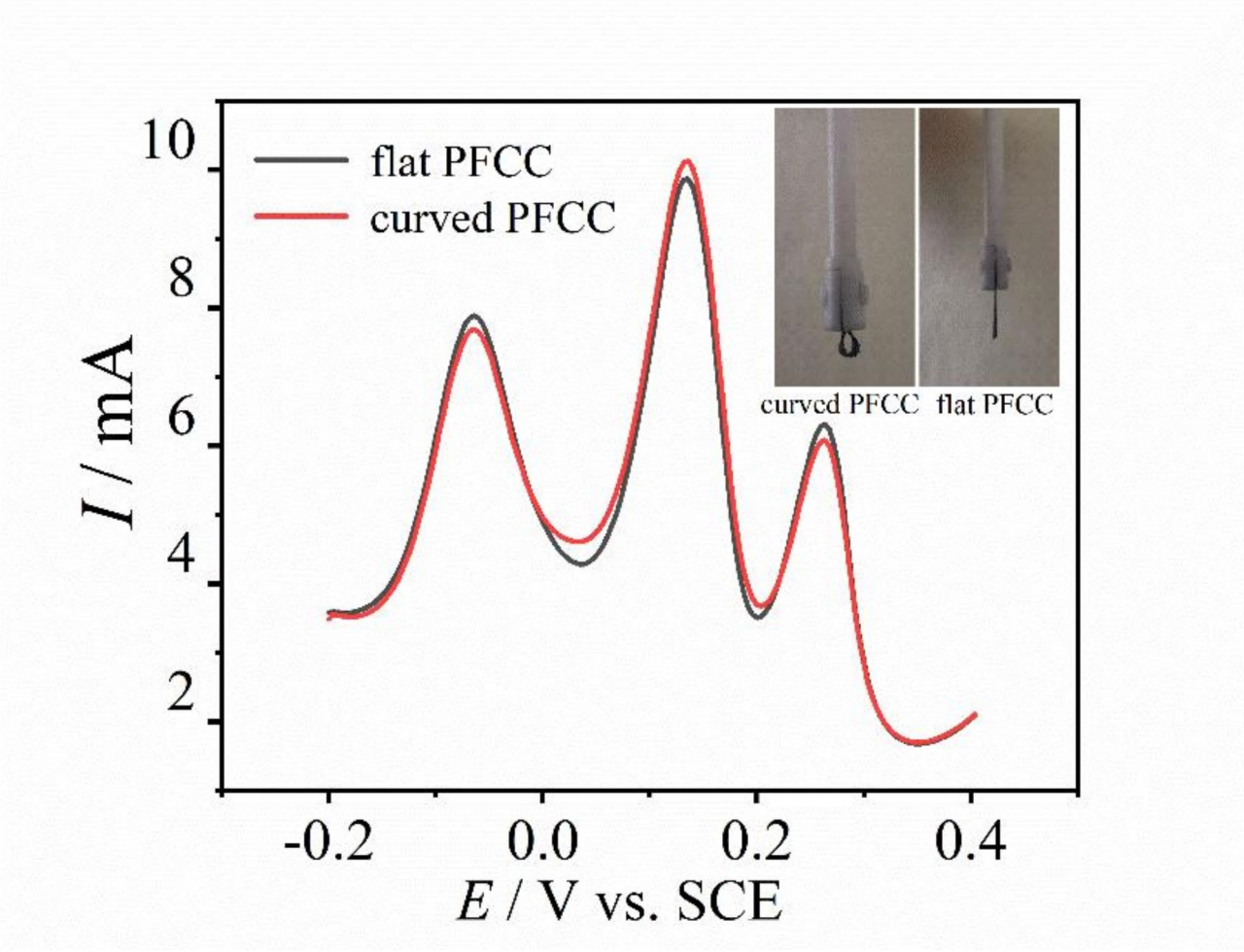

Fig. 11. DPV curves of the flat (**a**), curved (**b**) PFCC electrode.

response current to AA, DA, and UA remained at 90% of the initial current. The good stability of the PFCC electrodes is beneficial for practical applications.

Flexibility of PFCC

The development of flexible sensors with both high mechanical flexibility and sensitivity remains a significant challenge[23]. The excellent flexibility of CC makes it possible to manufacture flexible sensors. The flexibility of the sensor was evaluated by folding the PFCC at 180 °. Figure 11 shows the electrochemical response of flat or

Sample	Analyte	Detected (μM)	Added (μM)	Found (μM)	Recovery (%)	RSD(%)
1	AA	–	1000	1080	108	4.99
	DA	–	10	11.06	110.6	4.97
	UA	1.07	5	5.74	94.6	2.45
2	AA	–	1200	1120	93.3	4.47
	DA	-	8	7.39	92.4	2.92
	UA	1.07	8	9.07	100	2.65
3	AA	–	1500	1735	115.6	4.99
	DA	–	5	5.06	101.3	4.58
	UA	1.07	10	11.73	116.5	0.53

Table 5. Determination of AA, DA, and UA in fetal bovine serum ($n=3$).

curved PFCC to 1 mM AA, 20μM DA, and 20 μM UA. The current response of a curved PFCC is approximately 95% that of a flat PFCC, indicating that it possesses high mechanical flexibility and high sensitivity.

Detection of AA, DA, and UA in real sample

To verify the reliability of the practical application of PFCC, the AA, DA, and UA contents were determined in FBS. Different concentrations of AA, DA, and UA were added to the FBS sample diluted 100 times with 0.1 M PBS (pH = 7.0) for recovery experiments, and the experimental results are shown in Table 5. The recovery rate was between 92.4% and 116.5%, and the RSD obtained from three parallel tests for each concentration was less than 5%, indicating that the PFCC electrode has good reliability for detecting AA, DA, and UA.

Conclusions

In this study, three electrochemical methods were used to activate CC in 1 M $(NH_4)_2SO_4$ solution. Redox reactions occurred alternately on the electrode surface during the activation process using the CVA method. N and S were simultaneously doped on the surface of SFCC1 after activation, and the electrochemically active area of SFCC1 was the highest. The high surface area provided numerous active sites, and the doped N and S also provided additional active sites and enhanced its conductivity; consequently, SFCC1 exhibited excellent electrocatalytic performance for the oxidation of AA, DA, and UA. The activation of CC with CVA was also conducted in $(NH_4)_2HPO_4$ and NH_4Ac solutions. The oxidation of Ac^- inhibited the introduction of oxygen-containing functional groups and the enhancement of the surface area. Phosphate accelerated the doping of N; as a result, PFCC demonstrated the highest N doping level. Doping with N can improve the conductivity of PFCC, activate the hydroxy and amine groups in AA, DA, and UA, and accelerate the charge transfer of AA, DA, and UA. PFCC was used to detect AA, DA, and UA using the DPV method, which showed linear ranges of AA, DA, and UA concentrations of 0.1 to 2.1 mM, 0.5 to 11 μM, and 0.5 to 11 μM, respectively. The curved PFCC showed a similar response to AA, DA, and UA as that of the flat PFCC. The simultaneous determination of AA, DA, and UA in FBS showed a reliable recovery ratio. These results demonstrate that activating CC using the CVA method is an effective way to modulate its electrochemical performance and that PFCC is a promising material for flexible sensors to monitor AA, DA, and UA.

Data availability

The data that support the findings of this study are available from the corresponding author upon reasonable request.

Received: 27 June 2024; Accepted: 14 October 2024
Published online: 21 October 2024

References

1. Wang, H. et al. Three-dimensional g-C_3N_4/MWNTs/GO hybrid electrode as electrochemical sensor for simultaneous determination of ascorbic acid, dopamine and uric acid. *Analytica Chimica Acta 1211*. (2022).
2. Yang, L., Liu, D., Huang, J. & You, T. Simultaneous determination of dopamine, ascorbic acid and uric acid at electrochemically reduced graphene oxide modified electrode. *Sens. Actuators B* **193**, 166–172 (2014).
3. Sajid, M. et al. Chemically modified electrodes for electrochemical detection of dopamine in the presence of uric acid and ascorbic acid: a review. *TRAC Trends Anal. Chem.* **76**, 15–29 (2016).
4. Guan, J. F., Zou, J., Liu, Y. P., Jiang, X. Y. & Yu, J. G. Hybrid carbon nanotubes modified glassy carbon electrode for selective, sensitive and simultaneous detection of dopamine and uric acid. *Ecotoxicology and Environmental Safety*. 201 (2020).
5. You, Y. et al. Novel lanthanum vanadate-based nanocomposite for simultaneously electrochemical detection of dopamine and uric acid in fetal bovine serum. *Int. J. Biol. Macromol.* **195**, 346–355 (2022).
6. Ouedraogo, B., Baachaoui, S., Tall, A., Tapsoba, I. & Raouafi, N. Laser-induced graphene electrodes on polyimide membranes modified with gold nanoparticles for the simultaneous detection of dopamine and uric acid in human serum. *Microchim. Acta* **190**, 8 (2023).
7. Ma, T., Meng, J., Song, Q. & Wen, D. Superhydrophilic edge-rich graphene for the simultaneous and disposable sensing of dopamine, ascorbic acid, and uric acid. *J. Mater. Chem. B* **10**(7), 1094–1102 (2022).
8. Abbaspour, A., Khajehzadeh, A. & Ghaffarinejad, A. A simple and cost-effective method, as an appropriate alternative for visible spectrophotometry: development of a dopamine biosensor. *Analyst* **134**(8). (2009).

9. Teng, Y., Jia, X., Li, J. & Wang, E. Ratiometric fluorescence detection of tyrosinase activity and dopamine using thiolate-protected gold nanoclusters. *Anal. Chem.* **87**(9), 4897–4902 (2015).
10. Gao, J. et al. Electrodeposited NiO/graphene oxide nanocomposite: An enhanced voltammetric sensing platform for highly sensitive detection of uric acid, dopamine and ascorbic acid. *Journal of Electroanalytical Chemistry* **852** (2019).
11. Li, Y. & Lin, X. Simultaneous electroanalysis of dopamine, ascorbic acid and uric acid by poly (vinyl alcohol) covalently modified glassy carbon electrode. *Sens. Actuators B* **115** (1), 134–139 (2006).
12. Bahrami, E., Amini, R. & Vardak, S. Electrochemical detection of dopamine via pencil graphite electrodes modified by Cu/Cu_xO nanoparticles. *J. Alloys Compd.* **855** (2021).
13. Xiao, C. et al. Hollow nitrogen-doped carbon microspheres pyrolyzed from self-polymerized dopamine and its application in simultaneous electrochemical determination of uric acid, ascorbic acid and dopamine. *Biosens. Bioelectron.* **26**(6), 2934–2939 (2011).
14. Li, X. et al. Amperometric sensing of ascorbic acid by using a glassy carbon electrode modified with mesoporous carbon nanorods. *Microchim. Acta* **185**(10) (2018).
15. Sun, C. L. et al. Application of nanoporous core–shell structured multi-walled carbon nanotube–graphene oxide nanoribbons in electrochemical biosensors. *Microchemical Journal* **179** (2022).
16. Chu, Z. et al. Et. Al, Construction of a nano dispersed Cr/Fe-polycrystalline sensor via high-energy mechanochemistry for simultaneous electrochemical determination of dopamine and uric acid. *Microchim. Acta* **190**(3). (2023).
17. Wu, P. et al. $MnFe_2O_4/MoS_2$ nanocomposite as Oxidase-like for electrochemical simultaneous detection of ascorbic acid, dopamine and uric acid. *Microchemical Journal* **181** (2022).
18. Xi, X. et al. Et. Al, manipulating the sensitivity and selectivity of OECT-Based biosensors via the Surface Engineering of Carbon Cloth Gate electrodes. *Adv. Funct. Mater.* **30**(4) (2019).
19. Wang, H. et al. Et. Al, Ultramicroporous carbon cloth for flexible energy storage with high areal capacitance. *Energy Storage Mater.* **7**, 216–221 (2017).
20. Singh, A. et al. Et. Al, tailored carbon materials (TCM) for enhancing photocatalytic degradation of polyaromatic hydrocarbons. *Prog. Mater. Sci.* **144**. (2024).
21. Zhang, J., Zhao, Z., Xia, Z. & Dai, L. A metal-free bifunctional electrocatalyst for oxygen reduction and oxygen evolution reactions. *Nat. Nanotechnol.* **10**(5), 444–452 (2015).
22. Yuan, F. et al. Recent advances in inorganic functional nanomaterials based flexible electrochemical sensors. *Talanta* **224** (2022).
23. Zazoum, B., Batoo, K. M. & Khan, M. A. A. Recent advances in flexible sensors and their applications. *Sensors* **22**, 12 (2022).
24. Jian, M. et al. Et. Al, Advanced carbon materials for flexible and wearable sensors. *Sci. China Mater.* **60**(11), 1026–1062 (2017).
25. Xu, M. et al. Et. Al, a novel flexible electrochemical glucose sensor based on gold nanoparticles/polyaniline arrays/carbon cloth electrode. *Sens. Actuators B* **252**, 1187–1193 (2017).
26. Batool, R. et al. Et. Al, fabrication of polydopamine decorated carbon cloth as support material to anchor CeO_2 nanoparticles for electrochemical detection of ethanol. *Microchim. Acta* **190** (5). (2023).
27. Li, R. et al. Simple high-temperature annealing affords commercial carbon cloth with enhanced electrochemical performance for highly sensitive detection of imidacloprid. *Journal of Pharmaceutical and Biomedical Analysis* **219** (2022).
28. Wang, G. et al. Et. Al, solid-state Supercapacitor based on activated Carbon Cloths exhibits excellent rate capability. *Adv. Mater.* **26** (17), 2676–2682 (2014).
29. Ye, D., Yu, Y., Tang, J., Liu, L. & Wu, Y. Electrochemical activation of carbon cloth in aqueous inorganic salt solution for superior capacitive performance. *Nanoscale* **8**(19), 10406–10414 (2016).
30. Wang, W. et al. Et. Al, a Novel Exfoliation Strategy to significantly boost the Energy Storage Capability of Commercial Carbon Cloth. *Adv. Mater.* **27**(23), 3572–3578 (2015).
31. Ding, S. et al. Electrochemically functionalized carbon cloth for simultaneous determination of ascorbic acid, dopamine, and uric acid. *Journal of Electroanalytical Chemistry* **915** (2022).
32. Zhang, Y. & Xu, Y. Simultaneous Electrochemical Dual-Electrode Exfoliation of Graphite toward Scalable Production of High-Quality Graphene. *Adv. Funct. Mater.* **29**, 37 (2019).
33. Lou, F. et al. One-step electrochemical synthesis of tunable nitrogen-doped graphene. *J. Mater. Chem. A* **4**(4), 1233–1243 (2016).
34. Yang, Y. et al. Et. Al, Electrochemical exfoliation of Graphite into Nitrogen-doped Graphene in Glycine Solution and its Energy Storage properties. *Electrochim. Acta* **204**, 100–107 (2016).
35. Momodu, D. et al. Et. Al, mixed-acid intercalation for synthesis of a high conductivity electrochemically exfoliated graphene. *Carbon* **171**, 130–141 (2021).
36. Shayesteh Zeraati, A., Sharif, F., Aliabadian, E., Roberts, E. P. L. & Sundararaj, U. Co-doped electrochemically exfoliated Graphene/Polymer nanocomposites with high dielectric constant and low dielectric loss for Flexible Dielectrics and Charge Storage. *ACS Appl. Nano Mater.* **3**(5), 4512–4521 (2020).
37. Liu, F. et al. Et. Al, one-step electrochemical strategy for in-situ synthesis of S,N-codoped graphene as metal-free catalyst for oxygen reduction reaction. *Carbon* **134**, 316–325 (2018).
38. Gondosiswanto, R., Lu, X. & Zhao, C. Preparation of Metal-Free Nitrogen-Doped Graphene Via Direct Electrochemical exfoliation of Graphite in ammonium nitrate. *Aust. J. Chem.* **68**(5) (2015).
39. Gu, S. Y., Hsieh, C. T., Yuan, J. Y., Hsueh, J. H. & Gandomi, Y. A. Amino-functionalization of graphene nanosheets by electrochemical exfoliation technique. *Diam. Relat. Mater.* **87**, 99–106 (2018).
40. Sharif, F. et al. Et. Al, synthesis of a high-temperature stable electrochemically exfoliated graphene. *Carbon* **157**, 681–692 (2020).
41. Raj, C. J. et al. Et. Al, Sonoelectrochemical exfoliation of graphene in various electrolytic environments and their structural and electrochemical properties. *Carbon* **184**, 266–276 (2021).
42. Eda, G., Mattevi, C., Yamaguchi, H., Kim, H. & Chhowalla, M. Insulator to Semimetal Transition in Graphene Oxide. *J. Phys. Chem. C* **113**(35), 15768–15771 (2009).
43. Chen, S. et al. Et. Al, boosting electrocatalytic activity for CO_2 reduction on nitrogen-doped carbon catalysts by co-doping with phosphorus. *J. Energy Chem.* **54**, 143–150 (2021).
44. Pan, T. et al. Metal-free porous nitrogen-doped carbon nanotubes for enhanced oxygen reduction and evolution reactions. *Sci. Bull.* **61**(11), 889–896 (2016).
45. Li, S. M. et al. Et. Al, controllable synthesis of nitrogen-doped graphene and its effect on the simultaneous electrochemical determination of ascorbic acid, dopamine, and uric acid. *Carbon* **59**, 418–429 (2013).
46. Xing, B. et al. An insight into N,S-codoped activated carbon for the catalytic persulfate oxidation of organic pollutions in water: Effect of surface functionalization. *Applied Catalysis A: General* **602** (2020).
47. Matsoso, B. J. et al. The effect of N-configurations on selective detection of dopamine in the presence of uric and ascorbic acids using surfactant-free N-graphene modified ITO electrodes. *Electrochim. Acta* **286**, 29–38 (2018).
48. Gao, W. et al. One-step pyrolytic synthesis of Nitrogen and Sulfur Dual-Doped Porous Carbon with High Catalytic activity and good accessibility to small biomolecules. *ACS Appl. Mater. Interfaces* **6**(21), 19109–19117 (2014).
49. Kozbial, A., Trouba, C., Liu, H. T. & Li, L. Characterization of the intrinsic water wettability of Graphite using Contact Angle measurements: Effect of defects on static and dynamic contact angles. *Langmuir* **33**(4), 959–967 (2017).
50. Xia, Y. et al. et.al, Electrocatalytic activity enhancement of N,P-doped carbon nanosheets derived from polymerizable ionic liquids. *J. Appl. Electrochem.* **51**(4), 669–679 (2021).

51. Zhang, H. et al. Self-assembly synthesis of a hierarchical structure using hollow nitrogen-doped carbon spheres as spacers to separate the reduced graphene oxide for simultaneous electrochemical determination of ascorbic acid, dopamine and uric acid. *Anal. Methods* **5**, 14 (2013).
52. Gai, P. et al. Et. Al, simultaneous electrochemical detection of ascorbic acid, dopamine and uric acid based on nitrogen doped porous carbon nanopolyhedra. *J. Mater. Chem. B* **1**(21) (2013).
53. Huang, H. et al. Et. Al, Electrochemical sensor based on a nanocomposite prepared from $TmPO_4$ and graphene oxide for simultaneous voltammetric detection of ascorbic acid, dopamine and uric acid. *Microchim. Acta* **186**(3) (2019).
54. Zhang, X., Zhang, Y. C. & Ma, L. X. One-pot facile fabrication of graphene-zinc oxide composite and its enhanced sensitivity for simultaneous electrochemical detection of ascorbic acid, dopamine and uric acid. *Sens. Actuators B* **227**, 488–496 (2016).
55. Jiang, G., Jiang, T., Zhou, H., Yao, J. & Kong, X. Preparation of N-doped carbon quantum dots for highly sensitive detection of dopamine by an electrochemical method. *RSC Adv.* **5**(12), 9064–9068 (2015).
56. Li, Q. et al. Morphology-dependent MnO_2/nitrogen-doped graphene nanocomposites for simultaneous detection of trace dopamine and uric acid. *Materials Science and Engineering: C* **109** (2020).
57. Adeel, M., Canzonieri, V., Daniele, S., Rizzolio, F. & Rahman, M. M. Organobase assisted synthesis of $Co(OH)_2$ nanosheets enriched with oxygen vacancies for nonenzymatic glucose sensing at physiological pH. *J. Ind. Eng. Chem.* **103**, 165–174 (2021).

Acknowledgements

We gratefully acknowledge financial support from the Fundamental Research Funds for the Central Universities, China (N170504022).

Author contributions

Lijun Bian wrote the main manuscript text. Xinglin Su prepared Figs. 1, 2, 3, 4, 5, 6, 7, 8, 9, 10 and 11. Jialu Wang prepared Tables 1, 2, 3, 4, 5. All authors reviewed the manuscript.

Declarations

Competing interests

The authors declare no competing interests.

Additional information

Supplementary Information The online version contains supplementary material available at https://doi.org/10.1038/s41598-024-76495-7.

Correspondence and requests for materials should be addressed to L.B.